Geochimica et Cosmochimica Acta, Vol. 69, No. 16, pp. 4117–4126, 2005

0016-7037/05 $30.00 + .00

doi:10.1016/j.gca.2005.02.004

Diagenetic Alteration of Magnetic Signals by Anaerobic Oxidation of Methane Related to a Change in Sedimentation Rate

Natascha Riedinger,[1,*] Kerstin Pfeifer,[1] Sabine Kasten,[1] Johanna Fredrika Lukina Garming,[1] Christoph Vogt,[1] and Christian Hensen[2]

[1]Fachbereich Geowissenschaften, Universität Bremen, Klagenfurter Str., 28359 Bremen, Germany
[2]IFM-GEOMAR-Leibniz-Institut für Meereswissenschaften, Wischhofstr. 1–3, 24148 Kiel, Germany

(*Received June* 29, 2004; *accepted in revised form February* 1, 2005)

Abstract—Geochemical and rock magnetic investigations of sediments from three sites on the continental margin off Argentina and Uruguay were carried out to study diagenetic alteration of iron minerals driven by anaerobic oxidation of methane (AOM). The western Argentine Basin represents a suitable sedimentary environment to study nonsteady-state processes because it is characterized by highly dynamic depositional conditions. Mineralogic and bulk solid phase data document that the sediment mainly consists of terrigenous material with high contents of iron minerals. As a typical feature of these deposits, distinct minima in magnetic susceptibility (κ) are observed. Pore water data reveal that these minima in susceptibility coincide with the current depth of the sulfate/methane transition (SMT) where HS^- is generated by the process of AOM. The released HS^- reacts with the abundant iron (oxyhydr)oxides resulting in the precipitation of iron sulfides accompanied by a nearly complete loss of magnetic susceptibility. Modeling of geochemical data suggest that the magnetic record in this area is highly influenced by a drastic change in mean sedimentation rate (SR) which occurred during the Pleistocene/Holocene transition. We assume that the strong decrease in mean SR encountered during this glacial/interglacial transition induced a fixation of the SMT at a specific depth. The stagnation has obviously enhanced diagenetic dissolution of iron (oxyhydr)oxides within a distinct sediment interval. This assumption was further substantiated by numerical modeling in which the mean SR was decreased from 100 cm kyr^{-1} during glacial times to 5 cm kyr^{-1} in the Holocene and the methane flux from below was fixed to a constant value. To obtain the observed geochemical and magnetic patterns, the SMT must remain at a fixed position for ~9000 yrs. This calculated value closely correlates to the timing of the Pleistocene/Holocene transition. The results of the model show additionally that a constant high mean SR would cause a concave-up profile of pore water sulfate under steady state conditions. *Copyright © 2005 Elsevier Ltd*

1. INTRODUCTION

Iron (oxyhydr)oxides are a common component of marine sediments (e.g., Canfield, 1989; Haese et al., 2000) and are important carriers of magnetostratigraphic and paleomagnetic information (Frederichs et al., 1999; Bleil, 2000). After deposition primary iron mineral assemblages pass through a sequence of early diagenetic zones in which the minerals undergo alterations. Strong modifications of iron (oxyhydr)oxides and rock magnetic properties during the early stages of diagenesis across the Fe redox boundary have been documented by numerous studies (Wilson, 1986; Tarduno and Wilkison, 1996; Funk et al., 2003a, 2003b; Reitz et al., 2004). The early diagenetic transformation of iron (oxyhydr)oxides in marine sediments is linked to different pathways. One important process is the reaction with hydrogen sulfide via sulfate reduction (Berner, 1970; Froelich et al., 1979; Canfield, 1989; Lovley, 1991; Haese et al., 1998). Besides sulfate reduction driven by the bacterial degradation of organic matter, which typically occurs at high rates in the upper layers of the sediment (Jørgensen, 1982; Ferdelman et al., 1999), the process which ultimately leads to the complete consumption of interstitial sulfate in marine sediments is the anaerobic oxidation of methane (AOM). This important biogeochemical process finds its geochemical expression in a characteristic sulfate/methane transition (SMT) typically located one to a few meters below the sediment surface. Sulfate reduction driven by AOM releases adequate amounts of hydrogen sulfide into the pore water (Barnes and Goldberg, 1976; Bernard, 1979; Blair and Aller, 1995; Borowski et al., 1996; Niewöhner et al., 1998; Jørgensen et al., 2004). The liberated hydrogen sulfide leads to diagenetic alteration of primary geochemical and geophysical properties and the formation of distinct secondary signals in the zone of AOM (Passier et al., 1998; Kasten et al., 2003; Neretin et al., 2004).

The extent of geochemical and magnetic overprint occurring at geochemical boundaries and reaction fronts, particularly in deeper sediments is poorly understood. An important geochemical process in the zone of AOM is the transformation of magnetic iron minerals (Kasten et al., 1998; Passier et al., 1998). One of the major minerals to carry remanent magnetism in sediments is the ferrimagnetic mineral (titano)magnetite. The conversion of magnetite to iron sulfides during sediment diagenesis is a major cause of the loss of the magnetostratigraphic record in marine sediments (Karlin and Levi, 1983, 1985; Channell and Hawthorne, 1990; Karlin, 1990; Passier et al., 1998; Channell and Stoner, 2002). Ferrimagnetic iron oxides can be altered to paramagnetic iron sulfides (Berner, 1970; Canfield et al., 1992) and the magnetic signal can change

* Author to whom correspondence should be addressed (nar@uni-bremen.de).

dramatically (Canfield and Berner, 1987; Channell and Hawthorne, 1990; Channell and Stoner, 2002). An often cited mechanism is the formation of the iron sulfide pyrite via an intermediate sulfide mineral such as greigite (Berner, 1967; Roberts and Turner, 1993). These latter minerals are ferrimagnetic and their preservation would lead to the formation of a strong secondary magnetic signal (Roberts and Turner, 1993; Kasten et al., 1998; Jiang et al., 2001; Neretin et al., 2004). Intermediate iron sulfides are metastable, but they can persist for a considerable period of time if hydrogen sulfide is entirely consumed (Berner, 1982; Kao et al., 2004). Pyrite is thermodynamically more stable and thus will be the end-member of the transformation from iron (oxyhydr)oxides to iron sulfides (Berner, 1970; Coleman and Raiswell, 1995). However, if hydrogen sulfide is present in pore water, the oxidation of iron monosulfides by hydrogen sulfide can form pyrite directly without a greigite intermediate (Morse and Cornwell, 1987; Rickard et al., 1995; Butler and Rickard, 2000). Therefore, the diagenetic formation of iron sulfides in aquatic sediments has a strong effect on the interpretation of paleomagnetic data (Roberts and Turner, 1993; Furukawa and Barnes, 1995; Neretin et al., 2004).

The continental margin off Argentina and Uruguay represents a suitable sedimentary environment to study nonsteady-state processes because it is characterized by highly dynamic depositional conditions (Ewing et al., 1971; Biscaye and Dasch, 1971; Ledbetter and Klaus, 1987; Hensen et al., 2000, 2003). The sediment has a high content of ferric iron minerals and specific variations in magnetic signals (Sachs and Ellwood, 1988). Extensive geochemical and geophysical studies were carried out by Hensen et al. (2003) on sediments from the western Argentine Basin. Focusing on the reconstruction of mainly modern sedimentary history, especially gravity-driven mass flows, gravity cores with nonsteady-state sulfate pore water profiles (concave, kink-, and s-types) were investigated. In this study, we present geochemical, magnetic, and mineralogic data for three sediment cores from the continental margin off Argentina and Uruguay. These coring sites are characterized by a rather homogeneous recent sedimentation and linear sulfate pore water profiles. We investigate the influence of depositional settings and AOM on the diagenetic overprint of iron (oxyhydr)oxides and the resulting change in the magnetic record, and we present results of numerical modeling of the processes involved.

2. MATERIALS AND METHODS

2.1. Location and Geologic Settings

The study area is located in the western South Atlantic on the continental margin off Argentina and Uruguay (Fig. 1). The investigated gravity cores (Table 1) were taken during expeditions M46/2 and M46/3 of the RV *Meteor* (Bleil et al., 2001; Schulz et al., 2001). The gravity cores were retrieved east of the Rio de la Plata at the western boundary of the Argentine Basin. Sedimentation in this area is controlled by two main processes: gravity-controlled sediment transport and strong current circulation (Ewing and Leonardi, 1971; Klaus and Ledbetter, 1988). Terrigenous input originates from the numerous fluvial tributaries along the coast of Argentina and Uruguay (Iriondo, 1984; Piccolo and Perillo, 1999). The sediments are transported directly down-slope along the western margin of the Argentine Basin by gravity-controlled processes (Ewing et al., 1971; Biscay and Dasch, 1971; Klaus and Ledbetter, 1988; Sachs and Ellwood, 1988; Romero and Hensen, 2002; Hensen et al., 2003). These gravity-driven mass transports, such as debris flows and turbidity currents, are the main pathways of sediment supply into the deeper basin. The second important process controlling sedimentation in this area is the action of strong currents along the continental margin. The currents in the upper water column are the southward-flowing Brazil Current and the northward flowing Malvinas (Falkland) Current (Peterson and Stramma, 1991). These two currents meet in the Brazil Malvinas Confluence (BMC), located in front of the Rio de la Plata. The confluence of the two different water masses leads to an increase in primary production over a large area (Antoine et al., 1996; Behrenfeld and Falkowski, 1997), which results in relatively high inputs of organic carbon into the sediment. The suspended load of the Rio de la Plata is carried by northerly currents and thus forms a tongue of fine-grained sediment which is deposited parallel to the shore line off the coast of Uruguay (Ewing and Lonardo, 1971; Ledbetter and Klaus, 1987; Frenz et al., 2003). Between depths of 2000 and 4000 m, the water column is governed by the southward-flowing North Atlantic Deep Water (NADW). Below 4000 m, the strong currents carry Antarctic Bottom Water (AABW) to the north. These currents flow parallel to the continental margin, supplying benthic diatoms from higher latitudes (Romero and Hensen, 2002). The AABW dominates the transport of predominantly fine-grained sediment below 4000 m water depth. The

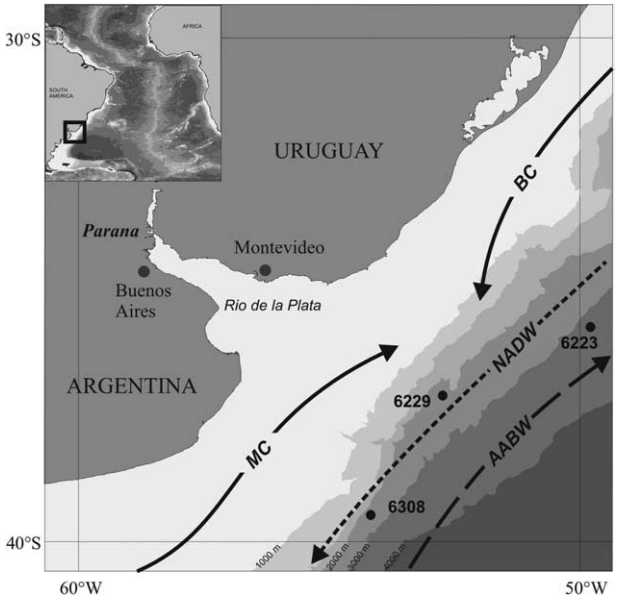

Fig. 1. Location map of the study area offshore of the Rio de la Plata. Arrows indicate simplified pathways of the main currents (solid line presents the surface-water currents MC (Malvinas Current) and BC (Brazil Current), and the lower-level and bottom-water currents are marked by dashed lines: NADW = North Atlantic Depth Water; AABW = Antarctic Bottom Water.

Table 1. Studied gravity cores with the location and water depth.

Station	Longitude [W]	Latitude [S]	Water Depth [m]	Core Length [m]
GeoB 6223-6	49°40.86′	35°44.42′	4280	8.67
GeoB 6223-5[a]	49°40.86′	35°44.43′	4280	8.15
GeoB 6229-6	52°39.00′	37°12.41′	3446	9.50
GeoB 6308-4	53°08.70′	39°10.00′	3620	11.66

[a] Core GeoB 6223-5 is the parallel core at site GeoB 6223 subjected to magnetic analysis.

currents winnow and entrain sediments deposited by gravity-controlled mass flows, and the fine material is transported into the deep basin (Groot et al., 1967; Ewing et al., 1971; Ledbetter and Klaus, 1987; Sachs and Ellwood, 1988).

The composition of the sediments in the study area is characterized by low calcium carbonate concentrations, but with relatively high amounts of organic carbon, biogenic opal, and iron (oxyhydr)oxides. Due to the sediment composition and the highly dynamic sedimentary conditions, few to no reliable stratigraphic information for this region exists (Romero and Hensen, 2002; Hensen et al., 2003).

2.2. Sampling

To prevent warming of the sediments after retrieval on board, all core segments were immediately placed in a cooling laboratory and were maintained at a temperature of ~4°C. Gravity cores were cut into 1-m segments on deck, and syringe samples were taken from the bottom of every segment for methane analysis. Higher-resolution sampling for methane was carried out in the cooling room by sawing 4 × 4 cm rectangles into the PVC liner. Syringe samples of 5 mL of sediment were taken every 20 to 25 cm. For hydrogen sulfide analyses at higher concentrations, 1 mL subsamples of the pore water were added to a ZnAc-solution to fix all hydrogen sulfide present as ZnS (see also Hensen et al., 2003).

Within the first two days after recovery, gravity cores were cut lengthwise into two halves and processed within a glove box under argon atmosphere. Conductivity and temperature were measured on the archive halves. On the working halves, pH and E_H were determined by punch-in electrodes, and sediment samples were taken every 25 cm for pressure filtration. Solid phase samples for total digestions, sequential extractions, and mineralogical analyses were taken at 10 cm intervals and kept in gas-tight glass bottles under argon atmosphere. The storage temperature for all sediments was −20°C to avoid dissimilatory oxidation of reduced species. Teflon squeezers were used for pressure filtration. The squeezers were operated with argon at a pressure that was gradually increased up to 5 bar. The pore water was retrieved through 0.2 μm cellulose acetate membrane filters.

2.3. Pore Water Analysis

The parameters hydrogen sulfide, sulfate, alkalinity, phosphate, and iron (Fe^{2+}) were determined by standard methods, as described in detail by Schulz (2000), within a few hours after retrieval of the pore water. All further analyses were carried out at the University of Bremen. Methane was measured with a gas chromatograph (Varian 3400), equipped with a splitless injector, by injecting 20 μL of the headspace gas. The concentrations were subsequently corrected for sediment porosity. Aliquots of the remaining pore water were diluted and acidified with HNO_3 for determination of cations using atomic absorption spectrometry (AAS; Unicam Solaar 989 QZ) and inductively coupled plasma atomic emission spectrometry (ICP-AES; Perkin Elmer Optima 3000 RL) techniques. For further information regarding analytical methods and devices, we refer to the homepage of the University of Bremen Geochemistry Group at http://www.geochemie.uni-bremen.de.

2.4. Solid Phase Analysis

All solid phase analyses were performed on anoxic subsamples. For total digestion, the samples were freeze-dried and homogenized in an agate mortar. About 50 mg of the sediment was digested in a microwave system (MLS-MEGA II and MLS-ETHOS 1600) and was treated with a mixture of 3 mL HNO_3, 2 mL HF, and 2 mL HCl. Dissolution of the sediments was performed at 200°C at a pressure of 30 bar. The solution was fully evaporated, redissolved with 0.5 mL HNO_3 and 4.5 mL deionized water (MilliQ) and homogenized. Finally, the solution was filled up to 50 mL with MilliQ. Major and minor elements were measured by ICP-AES. The accuracy of the measurements was verified using standard reference material USGS-MAG-1. The reference material element concentrations were within certified ranges. The precision of ICP-AES analyses was better than 3%.

The concentrations of reactive Fe phases were determined following the method described by Haese et al. (2000). In the first step, 150–250 mg of the wet sample was treated with 20 mL of an ascorbate solution (a weak reducing agent) containing sodium citrate, sodium carbonate, and ascorbate acid and extracted over 24 hours. In the second step, the ascorbate residuum was treated with 20 mL of a dithionite solution consisting of acetic acid, sodium citrate, and sodium dithionite and kept in suspension for one hour. The extractions of ascorbate and dithionite were diluted 1:10 and measured by ICP-AES. Standards were prepared using the corresponding matrix.

For the determination of inorganic carbon (IC) and total organic carbon (TOC) contents, freeze-dried and homogenized samples of cores GeoB 6229-6 and GeoB 6308-4 were measured using a LECO CS-300 carbon sulfur analyzer. For organic carbon, the samples were treated with 12.5% HCl, washed two times with MilliQ and dried at 60°C. The accuracy, checked by marble standards, was ±3%. The samples of core GeoB 6223-6 were measured using a Shimadzu TOC with SSM 5000A carbon analyzer. Inorganic carbon was measured by adding 35% phosphoric acid to the sample and heating up to 250°C. The accuracy is ±3%, and the limit of detection is below 0.05% for a 100 mg sample.

The data set of pore water and solid phase measurements is available via the geological data network Pangaea (http://www.pangaea.de).

2.5. Mineral Analysis

Mineral identification was carried out by X-ray diffraction (XRD), which was performed at a few selected depths of core GeoB 6229-6 (75, 375, 545, 675, and 725 cm) using Philips X'Change (Cu-tube) with fixed divergence slit. The measurement was carried out with a first angle of 3° 2Θ and a last angle of 100° 2Θ. The step size was 0.02° 2Θ, with measurement time of 12 s/step. Samples from core GeoB 6223-6 (255, 525, 655 cm) and core GeoB 6308-4 (555 and 655 cm) were measured using an X'Pert Pro MD, X'Celerator detector system, with a step size of 0.033° 2Θ, and the calculated time per step was 219.7 s. Quantification of the mineral content was carried out with QUAX (for further information see Vogt et al., 2002). Scanning electron microscope (SEM) analysis was performed on selected samples.

2.6. Magnetic Susceptibility Measurement

The magnetic susceptibility data for site GeoB 6223 were obtained on the parallel core GeoB 6223-5 on board the RV *Meteor*. Determination of susceptibility on the archive halves of the gravity cores GeoB 6229-6 and GeoB 6308-4 took place at the University of Bremen. The susceptibility measurements were performed using a nonmagnetic automated core conveyor system equipped with a commercial Bartington Instruments MS2 susceptibility meter with an F-type spot sensor. The measurement interval was 2 cm and 1 cm, respectively.

2.7. Geochemical Modeling

AOM and the associated diagenetic processes were simulated with the nonsteady-state transport and reaction model CoTReM. A detailed description of this computer software is given in the CoTReM User's Guide (Adler et al., 2000; http://www.geochemie.uni-bremen.de/cotrem.html) and by Adler et al. (2001). The upper 20 m of the sediment (model area) was subdivided into cells of 5 cm thickness. The time-step to fulfill numerical stability was set to 10^{-1} yr, and the porosity of the sediment was set to 75%. Transport mechanisms were molecular diffusion (D_s) for all solutes in the pore water and the sedimentation rate (SR) for the solid phase and pore water. Diffusion coefficients were corrected for tortuosity (Boudreau, 1997) using a temperature of 2°C. The bottom water concentration of species defines the upper boundary condition. The lower boundary is defined as an open/transmissive boundary, which means that the gradient of the last two cells is extrapolated to allow diffusion across the boundary. For methane, a fixed concentration was defined at the lower boundary that creates the gradient necessary to simulate the measured influx of methane into the model area from below. For geochemical reactions, 0th-order kinetics were used by defining maximum reaction rates. These rates are used as long as the educt species are available in sufficient amounts. If the amount decreases, the rates were automatically reduced to the available amount of reactants in each cell to avoid negative concentrations (for

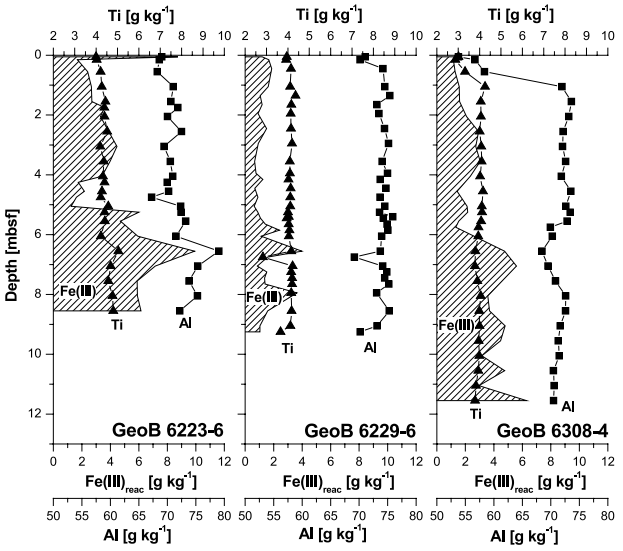

Fig. 2. Solid phase data for Al (solid squares) and Ti (solid triangles) indicating the dominance of terrigenous input. The cross-hatched area indicates the amount of reactive Fe(III) phases.

further details see Hensen et al., 2003). All input parameters are given in the respective section below.

3. RESULTS AND DISCUSSION

3.1. Sediment Composition

Sediment composition and grain size are two important parameters that affect diagenetic processes (Roberts and Turner, 1993). These attributes vary in all three cores. Whereas the sediment of cores GeoB 6229 and GeoB 6308 is quite variable in grain size, the sediment in core GeoB 6223-6 is rather fine-grained, as identified macroscopically and by SEM. At all sites, the composition of the sediment is dominated by lithogenic components, as indicated by the major mineral assemblages of selected samples from all three cores (20–28 wt% quartz, 18–35 wt% feldspar, and 23–44 wt% phyllosilicates). The lowest amounts of phyllosilicates were found at site GeoB 6308. Additionally, solid phase concentrations of Al and Ti indicate a high terrigenous input (Fig. 2). Total concentrations of Al and Ti positively correlate in sediments of the southernmost site GeoB 6308-4 ($R^2 = 0.93$), which is not the case for the other two sites (GeoB 6229-6 $R^2 = 0.60$ and GeoB 6223-6 $R^2 = 0.75$). We attribute this finding to variable depositional processes. The comparatively high content of glauconite (3–17 wt%) detected by XRD in the sediment from all three cores gives evidence for mass flow deposition events. In general, glauconite in recent sediment is an indicator of slow rates of clastic deposition in shallow marine environments (Odin and Matter, 1981; Harris and Whiting, 2000). The presence of this mineral at all three sites suggests erosion of near-shore/shelf sediments and redeposition at greater water depths on the continental slope. A further characteristic component of the sediments of this area is the relatively high amount (up to 1 wt%) of reactive iron (oxyhydr)oxides (Fig. 2).

All three cores display a distinct change in sediment composition in the uppermost section. Total organic carbon (TOC) reaches values of up to 1.1 wt% close to the sediment surface, while the mean content for the deeper sediment is ~0.7 wt% (Fig. 3). Correspondingly, calcium carbonate also has the highest overall concentrations in the uppermost sediments. The calcium carbonate contents are generally low and are well correlated with the total concentration of calcium obtained from acid digestion. The lack of carbonate in the deepest core GeoB 6223-6 can be due to the depositional system, e.g., dilution by terrigenous input, or due to its depth lying below the lysocline resulting in dissolution of carbonate (Archer, 1996; Frenz et al., 2003). At site GeoB 6229, $CaCO_3$ concentrations of up to 5 wt% were determined, and, at the southernmost site GeoB 6308, high $CaCO_3$ contents of up to 18 wt% are found in the uppermost layer (Fig. 3). A similar transition from terrigenous-dominated to carbonate-enriched sediments in the upper sediment layers is also found in sediments of the Amazon Fan (e.g., core GeoB 1514-6 of Kasten et al., 1998). In these sediments, a sedimentation change is found at ~60 cm, with $CaCO_3$ gradually increasing upward. While the glacial sedimentation rate for the Amazon Fan area amounts to a few meters per kyr (Flood et al., 1995), stratigraphic data for the upper 35 cm at site GeoB 1514 indicate a Holocene age with an SR of 3.5 cm kyr^{-1} (Schneider et al., 1991). A similar transition from terrigenous-dominated to more calcareous sediments in the upper sediment layers for the investigated sites would suggest a Holocene SR of ~3 to ~7 cm kyr^{-1}. This is in good agreement with unpublished stratigraphic data by O. Romero (personal communication) from Argentine Basin sites (e.g., GeoB 6340 at 44°54.95′S, 58°05.78′W, water depth 2785 m), which reveal an SR of a few cm per kyr in the Holocene. Although the mean SR in the investigated area is not the same as for the Amazon Fan, similar patterns in sediment composi-

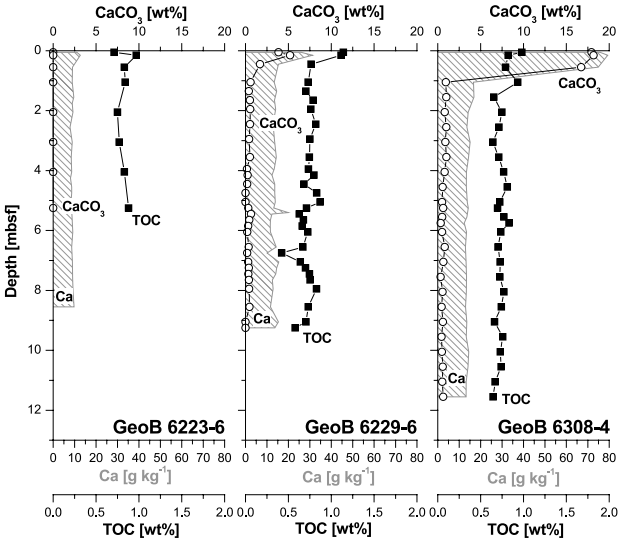

Fig. 3. Solid phase concentrations of total Ca (cross-hatched area), calcium carbonate (open circles), and total organic carbon (TOC, solid squares). The TOC in the upper layer of core GeoB 6308-4 is diluted by the higher amount of $CaCO_3$. There is no measurable carbonate in the sediment of core GeoB 6223-6, but there is a higher organic carbon content in the uppermost centimeters before it decreases toward the sediment surface.

tion are consistent with a comparable decrease in mean SR during the glacial/interglacial transition.

3.2. Diagenetic Alteration

The sulfate pore water profiles for all three studied cores show a linear decrease with depth, which indicates a currently steady-state situation (Fig. 4). The SMT is located between 5 and 5.5 mbsf (meters below seafloor) in each case. In cores GeoB 6229-6 and GeoB 6308-4, excess hydrogen sulfide could be detected at depths of 4–7 and 4–6 mbsf, respectively. The sulfidic sediment intervals are characterized by distinct minima in magnetic susceptibility (Fig. 4). Based on the pore water data, we suggest that the characteristic decrease in magnetic susceptibility (κ), which is a widespread phenomenon in sediments of the continental margin off Argentina and Uruguay, is caused by diagenetic processes within the zone of AOM. Except for the decrease in magnetic susceptibility in the uppermost centimeters of core GeoB 6308-4, which is due to dilution by $CaCO_3$, we attribute the decrease in magnetic susceptibility to the reduction of iron (oxyhydr)oxides by hydrogen sulfide and subsequent formation of iron sulfides as described by Karlin and Levi (1983) and Channell and Hawthorne (1990).

Because of the current relatively high fluxes of methane and sulfate into the SMT at all three sites (Fig. 4), we suggest that deep sulfate reduction is primarily driven by AOM (Niewöhner et al., 1998). Thus, hydrogen sulfide is produced by a reaction of sulfate and methane (e.g., Barnes and Goldberg, 1976):

$$CH_4 + SO_4^{2-} \rightarrow + HCO_3^- + H_2O + HS^-\cdot \quad (1)$$

The species distribution of hydrogen sulfide is pH dependent (Pyzik and Sommer, 1981). Based on the measured pH values (7.2 to 8.0), we conclude that HS^- is the predominant hydrogen sulfide species in the sediment of the studied cores.

The concentration of measured reactive iron (oxyhydr)oxides for cores GeoB 6223-6 and GeoB 6308-4 is low (Fig. 2) in the interval where magnetic susceptibility data show a minimum (Fig. 4). In this zone, the iron (oxyhydr)oxides are almost completely reduced and only relict concentrations are left. For the process of iron (oxyhydr)oxide reduction, the assumed reactions for lepidocrocite (Eqn. 2) (as an example for iron (oxyhydr)oxides) and for magnetite (Eqn. 3) are

$$2FeOOH + HS^- + 5H^+ \rightarrow 2Fe^{2+} + S^0 + 4H_2O \quad (2)$$

$$Fe_3O_4 + HS^- + 7H^+ \rightarrow 3Fe^{2+} + S^0 + 4H_2O\cdot \quad (3)$$

The available dissolved ferrous iron reacts directly with HS^- (Berner, 1970; Pyzik and Sommer, 1981) according to the equation:

$$Fe^{2+} + HS^- \rightarrow FeS_{(s)} + H^+\cdot \quad (4)$$

The precipitated amorphous iron sulfide is highly unstable and transforms rapidly to other iron sulfide phases (Schoonen and Barnes, 1991). Morse (2002) discussed that the oxidation of FeS by hydrogen sulfide (Eqn. 5) is the faster process compared with the oxidation by elemental sulfur as discussed by Berner (1970). In addition, Rickard (1997) pointed out that pyrite formation through oxidation by HS^- is thermodynamically favored:

$$FeS_{(s)} + HS^-_{(aq)} + H^+_{(aq)} \rightarrow FeS_{2(s)} + H_{2(g)} \quad (5)$$

In contrast to the intermediate iron sulfides, pyrrhotite ($Fe_{x-1}S$) and greigite (Fe_3S_4), the iron disulfide pyrite is paramagnetic and therefore has a low magnetic susceptibility and does not contribute to the remanent magnetization of a sediment. Because both pyrite and marcasite are paramagnetic, we term all iron disulfides as pyrite for simplicity. Thus, the dissolution of magnetite and the precipitation of pyrite would cause a strong decrease in magnetic susceptibility. Such a decrease of the magnetic signal can be observed in the susceptibility (κ) at all three sites (Fig. 4).

3.3. Magnetic Susceptibility Profiles

We have explained the mechanisms of alteration of iron (oxyhydr)oxides to iron sulfides within the zone of AOM, but we still have to explain the occurrence of iron (oxyhydr)oxides below the SMT. We assume that there are only a few possible processes that can cause a decrease of iron (oxyhydr)oxides limited to the zone of AOM and that leads to a localized minimum in magnetic susceptibility.

One process would be the reoxidation of ferrous iron below the sulfidic zone. The oxidation could be driven by Mn(II) released during reduction of Mn-oxides (Aller and Rude, 1988; Postma and Appelo, 2000; Schippers and Jørgensen, 2001). This process could explain the existence of iron (oxyhydr)oxides below the SMT where no hydrogen sulfide is present. Detailed rock magnetic and SEM analyses performed on magnetic minerals of samples from core GeoB 6229-6 by Garming

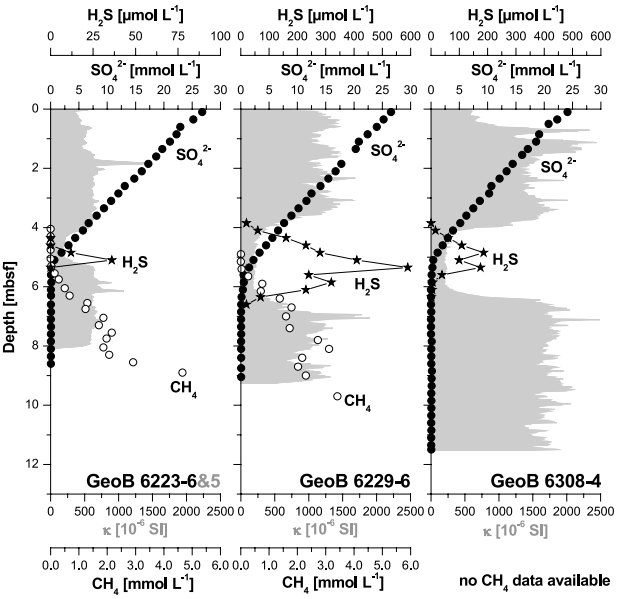

Fig. 4. Sulfate (solid circles), methane (open circles), and sulfide (solid stars) pore water profiles (pore water data for methane, sulfate, and sulfide for core GeoB 6223-6 and sulfate for core GeoB 6229-6 are taken from Hensen et al., 2003) and the magnetic susceptibility (gray area) (note that the offset for data from core GeoB 6223-5 is probably due to the measurements coming from a parallel core). Except for the decrease in magnetic susceptibility at the top of the core GeoB 6308-4, due to the dilution by higher carbonate concentrations, the decrease in susceptibility is restricted to the sulfidic zone.

Table 2. Parameters used in modeling of magnetic susceptibility profiles for different sedimentation rates.

Parameters		
Model area[a]:	20 m	
Cell discretization:	5 cm	
Time step:	1×10^{-1} yr	
Sediment porosity:	75%	
Temperature:	2°C	
Input concentration		
Magnetite (Fe_3O_4):	1 wt%	
	Upper boundary	Lower boundary
Sulfate (SO_4^{2-}):	26 mmol L^{-1}	0 mmol L^{-1}
Methane (CH_4):	0 mmol L^{-1}	45 mmol L^{-1}

[a] The model area is the sediment column incorporated in the approach.

et al. (2005) reveal that the magnetic mineral assemblages above and below the zone of AOM are similar and that the authigenic formation of iron oxides can therefore be excluded.

Another process that could potentially cause a distinct loss in magnetic susceptibility in the zone of AOM is a variation in the parameters controlling the position of the SMT. The depth at which the SMT is established is driven mainly by the upward flux of methane and the downward diffusion of sulfate, which is directly influenced by the SR. We simulated different scenarios with the numerical model CoTReM to investigate whether a constant mean SR alone can lead to the observed profiles of magnetic susceptibility. Under steady-state conditions prevailing over a long period of time, with continuous sedimentation and no change in the upward flux of methane, the zone of AOM would keep a fixed offset with respect to the sediment surface (Borowski et al., 1996; Kasten et al., 2003). This process would lead to a continuous reduction of iron (oxyhydr)oxides within the SMT and below. The degree of reduction to which every sediment layer is subject would thereby be coupled to the rate at which the zone of AOM moves upward as a function of SR. The dissolution rate is dependent on the reactivity of the iron (oxyhydr)oxides and their grain size, and the time period over which they are in contact with hydrogen sulfide (Pyzik and Sommer, 1981; Karlin and Levi, 1983, 1985; Canfield and Berner, 1987; Canfield, 1992; Roberts and Turner, 1993).

Hensen et al. (2003) give a detailed description for reaction kinetics of hydrogen sulfide with a continuum of different Fe(III)-phases. The reaction rates are sensitive to dissolved Fe and HS^- in the model approach because HS^- is involved in two reactions (Eqns. 3 and 4). For simplicity, we consider only magnetite (Fe_3O_4) and adapt a maximum reaction rate of 3×10^{-5} mol L^{-1} yr^{-1} to account for the measured hydrogen sulfide concentration compared to rates of between 5.5×10^{-6} mol L^{-1} yr^{-1} and 1.2×10^{-4} mol L^{-1} yr^{-1} in Hensen et al. (2003). The initial concentration of Fe_3O_4 is set to 1 wt%, which is reduced to iron monosulfide (FeS) in the sulfidic zone. A compilation of input parameters for all simulation runs is given in Table 2, where the lower boundary is defined at a model depth of 20 m (whereas the figures are only displayed to a depth of 13 m). During simulation of a relatively low mean SR of 5 cm kyr^{-1} (Fig. 5a), the SMT moves slowly upward, resulting in the complete transformation of the initially present magnetite into iron sulfides (Fig. 5b). In contrast, more rapid sedimentation can lead to the preservation of a considerable amount of magnetic iron oxides and therefore to a preservation of the magnetic record, as also discussed by Canfield and Berner (1987). Model runs with a high mean SR of 200 cm kyr^{-1} result in fast burial of magnetite (Fig. 6a), with reduction of only a small amount (~1/5) of Fe_3O_4 (Fig. 6b). These model runs demonstrate that the observed patterns cannot be formed under conditions of constant mean SR.

Different scenarios were modeled to assess the influence of variations in depositional and/or geochemical conditions on the position of the SMT. A sudden increase in the upward methane flux would push up the SMT and result in a concave-up sulfate pore water profile (Hensen et al., 2003; Kasten et al., 2003). At a constant high mean SR, this concave-up profile would remain and the observed linear sulfate profile would not be seen. At low mean SR, the SMT would move rapidly upward owing to the increased methane flux until a new steady state with a linear sulfate pore water profile is regained. But, as shown in the simulation of constant mean SR (Fig. 5a), at a low mean SR all

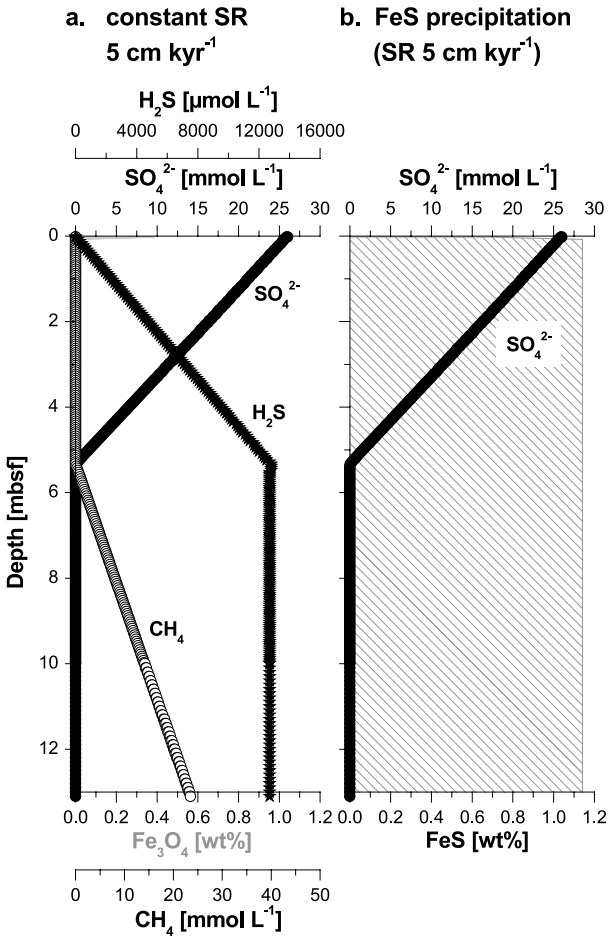

Fig. 5. Modeling results for diagenetic alteration of magnetite to iron monosulfide. (a) Sulfate, methane and sulfide profiles at a constant mean SR of 5 cm kyr^{-1}. (b) All iron (oxyhydr)oxides are altered into iron monosulfides.

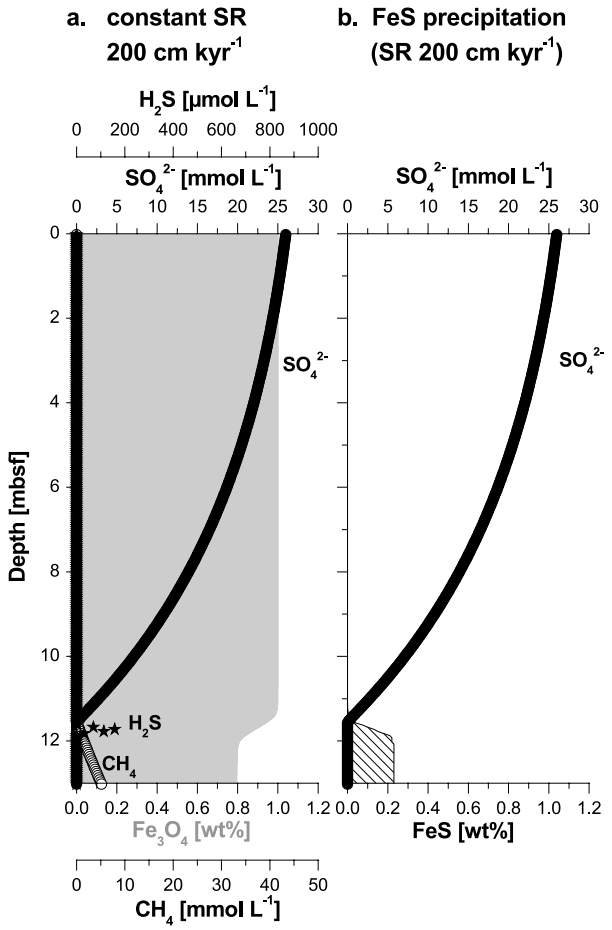

Fig. 6. Model results for a constant mean SR of 200 cm kyr^{-1}. (a) The high mean SR leads to good preservation of magnetite below the SMT. The pore water profile for sulfate shows a concave-up shape. (b) Only a small amount of iron sulfide is precipitated in this scenario.

available reactive iron (oxyhydr)oxide would be altered and thus the increased methane flux would not produce the observed localized magnetic susceptibility minimum.

After demonstrating that variations in the upward methane flux alone cannot produce the observed patterns, we simulated the effect of changing mean SR. Kasten et al. (1998) demonstrated that the strong decrease in SR for Amazon Fan sediments as a consequence of the glacial/interglacial transition was responsible for the fixation of the SMT for a prolonged period of time. To test whether the observed profiles of magnetic susceptibility could be explained by a drastic decrease in mean SR, we modeled scenarios of different mean SR with a constant methane flux over time. The history of sedimentary events for the three studied sites are not known in detail. We therefore assume, as the starting condition for the model, a high mean SR of 100 cm kyr^{-1} (Fig. 7a). This mean SR includes all possible mechanisms of sediment deposition. This mean SR is sufficiently high to limit the contact time between the iron oxides and the sulfidic pore water, and thus to alter only one third of the initially present iron oxides into iron sulfides. With a subsequent decrease in the rate of sedimentation to ~5 cm kyr^{-1}, estimated from $CaCO_3$ concentrations in the solid phase (see section 3.1), the SMT moves upward until a steady-state is regained (Fig. 7b). In this scenario, there is a complete transformation of all available iron oxides to iron monosulfides in the SMT and subsequently in the expending zone of excess hydrogen sulfide (Fig. 7c). This process causes a pronounced loss in magnetic susceptibility in a particular sediment interval. The time needed for the complete conversion of magnetite into iron sulfides in an interval of 2 m (e.g., GeoB 6308-4) is ~8000 yrs. Although the results of our approach are strongly dependent on the boundary parameters, the estimation correlates well with a change in mean SR at the glacial/interglacial transition.

A further interesting finding of the simulation is the concave-up sulfate profile at high constant mean SR. This shape of the sulfate profile has previously been described for nonsteady-state conditions such as an increased methane flux (Kasten et al., 2003), upward-directed advective flow (e.g., Aloisi et al., 2004), and transient diagenesis after a sedimentary event has occurred (Hensen et al., 2003). An example of a transient event is a single submarine slide event, which results in a kink-type profile (de Lange, 1983; Zabel and Schulz, 2001) that is smoothed to a concave-up and finally a linear profile by diffusion. As shown by our model outcome, the concave-up sulfate profile can also result from high mean SR under steady-state conditions. This could be explained by the high sulfate accumulation compared with the diffusion flux of sulfate.

3.4. Solid Phase Enrichment of Iron and Sulfur

For core GeoB 6308-4, the solid phase profiles of total iron and sulfur (Fig. 8) indicate an enrichment of iron sulfides

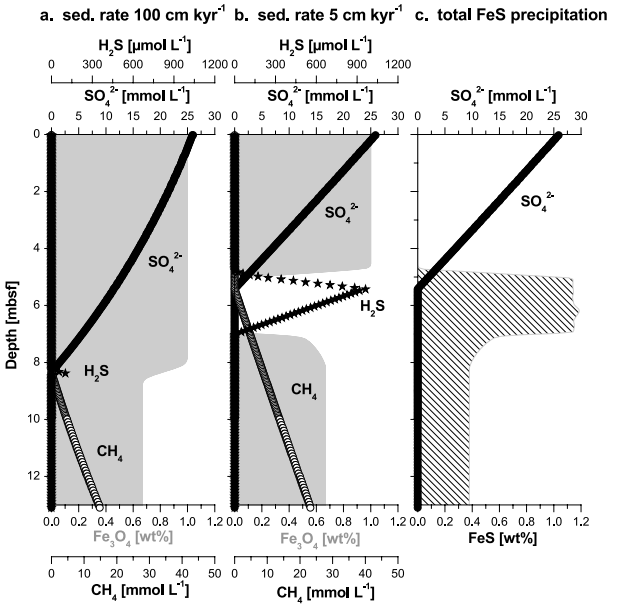

Fig. 7. Modeling results for diagenetic alteration of magnetite to iron monosulfide with a major change of mean SR (for sediment porosity of 75%). (a) A mean SR of 100 cm kyr^{-1} leads to reduction of only about one third of the Fe_3O_4. (b) If the mean SR is decreased to 5 cm kyr^{-1}, a time interval of ~8000 yrs is needed to reduce the total amount of magnetite for an interval of 2 m thickness. (c) The cross-hatched area indicates the total amount of precipitated monosulfides for the modeled scenario with change in mean SR.

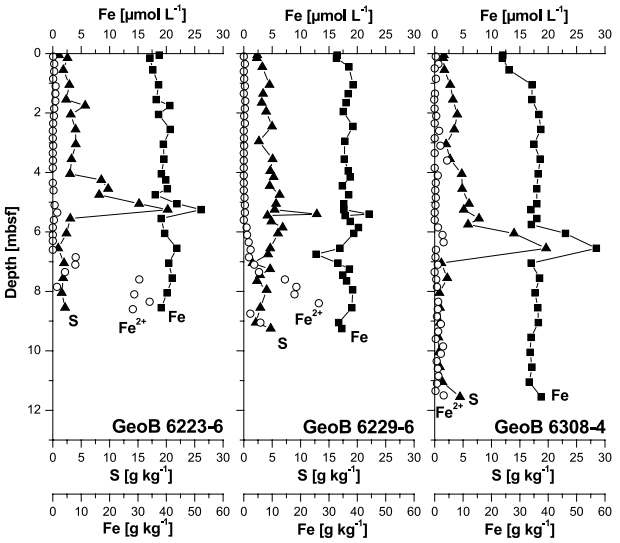

Fig. 8. Total sulfur (solid triangles) and total iron (solid squares) concentrations of the solid phase. Correlation of the iron and sulfur peak at sites GeoB 6223 and GeoB 6308 indicates an iron sulfide enrichment. The iron minimum in the sediment of core GeoB 6229-6 correlates with a turbidite sequence. Open circles indicate ferrous iron pore water concentrations.

between 6 and 7 mbsf. Similar solid phase peaks of total iron and sulfur are found at site GeoB 6223, where XRD analyses of the sample taken at 525 cm prove the presence of pyrite (2.5 wt%). The accumulation of authigenic iron sulfides within this distinct interval could be explained by diffusion of ferrous iron from below reacting with hydrogen sulfide (e.g., Kasten et al., 1998). At site GeoB 6223, ferrous iron is detected in pore water directly below the solid phase iron enrichment (Fig. 8). Another explanation for the enrichment of iron in the solid phase could be the consequence of an initial enrichment of iron (oxyhydr)oxides at this particular layer due to a sedimentary event. The iron (oxyhydr)oxides will be reduced and the ferrous iron can be transformed directly into iron sulfide. As the enrichment of total iron and sulfur in core GeoB 6308-4 is located below the distinct susceptibility minimum, we suggest that the reduction of the magnetic minerals ((titano)magnetite) has not yet taken place and that only the more reactive iron phases have been reduced.

Under the premise of a decrease in mean SR, and hence a fixation of the zone of AOM for a specific length of time, we calculated the time needed to produce the total amount of solid phase sulfur in the sediments of site GeoB 6223 at 525 cm and at site GeoB 6308 at 625 cm. The calculation is described in detail by Kasten et al. (1998). We simulated the enrichment of solid phase sulfur by downward diffusion of sulfate, assuming that the sulfur contained in the solid phase was fixed owing to the precipitation of iron sulfide as a result of hydrogen sulfide liberated by AOM. Assuming a linear sulfate pore water profile over the whole time of iron sulfide formation, the flux of pore water sulfate is calculated using Fick's first law, with a diffusion coefficient in free solution (D_0) for sulfate of 165 $cm^2\ yr^{-1}$ (after Iversen and Jørgensen, 1993). The sediment dry density averages 2.2 $g\ cm^{-3}$, and the temperature is 2°C. The presumed mean Holocene SR amounts to 5.0 cm kyr^{-1}. If we assume a porosity of 70% for the sediment of core GeoB 6223-6 and 75% for core GeoB 6308-4, the time needed to produce the measured sulfur peak would be ~9000 yrs. This calculated result is in good agreement with the outcome of the model above. Based on the model results, we suggest that the only scenario that produces the observed localized loss in magnetic susceptibility is a nonsteady-state diagenetic scenario involving a drastic decrease in mean SR, from a few hundred cm to ~5 cm per 1000 yrs, during the Pleistocene/Holocene transition leading to a fixation of the SMT for a period of 8000 to 9000 yrs.

4. CONCLUSIONS

A marked localized minimum in magnetic susceptibility in distinct sediment intervals of Argentine Basin deposits is observed, which correlates with the current position of the SMT. To explain the diagenetic impact of AOM on magnetic susceptibility, we modeled different geochemical and depositional scenarios. The model results indicate that the depletion of iron (oxyhydr)oxides and the resulting strong decrease in magnetic susceptibility within the sulfidic zone around the current depth of the SMT is an effect of the rather low and constant mean SR since the beginning of the Holocene, compared with the high mean SR of one to several meters per kyr during the last Glacial. The drastic change in mean SR results in a fixed or slow-moving SMT, which increases the time of contact between iron (oxyhydr)oxides and the liberated hydrogen sulfide, leading to enhanced dissolution of iron (oxyhydr)oxides and formation of the paramagnetic iron sulfide pyrite in this particular sediment layer. Furthermore, the results of the model indicate that a constant high mean SR is able to cause a concave-up pore water sulfate profile. Such concave-up sulfate profiles have been previously interpreted to result from either nonsteady-state depositional conditions or from upward-directed advective flow. In the scenarios that we have modeled, the concave-up sulfate profile would be a steady-state case. A low mean SR with a fixation of the SMT is necessary to produce an enrichment of iron and sulfur in the solid phase, as can be found in the sediment at sites GeoB 6223 and GeoB 6308. We calculated the time needed to produce the total amount of sulfur in the solid phase to be ~9000 yrs, which corresponds well with the estimation of the model and the Pleistocene/Holocene transition.

However, the stagnation of the SMT caused a loss of magnetic signal by diagenetic destruction of magnetite due to AOM. Another influence of AOM on sediment magnetism can be, e.g., a magnetic enhancement via growth of greigite. This important but different magnetic effect was described by Neretin et al. (2004). The two effects are both results of similar processes, except that pyritization seems to have been arrested in the study by Neretin et al. (2004), which has led to preservation of greigite nodules with magnetizations 10–100 times greater than surrounding sediments. The net result is that nonsteady-state diagenesis can have varying effects on the magnetic record. Thus, diagenetic transformation of iron oxides to iron sulfides in the zone of AOM that corresponds to a loss and new formation of magnetic signals should be considered in the interpretation of magnetic records.

Acknowledgments—We thank the captains and crews of the RV *Meteor* for their strong support during the two cruises M46/2 and M46/3. For technical assistance on board and in the home laboratory, we are indebted to S. Hinrichs, S. Siemer, K. Enneking, and S. Hessler. We

highly appreciate magnetic data provided by and discussions with T. Frederichs and SEM analyses carried out by H. Mai. Furthermore, we thank V. Heuer, K. Plewa, and M. Schweizer for laboratory support. F. Aspetsberger, K. Seiter, O. Romero, and M. Zabel are thanked for detailed comments on an earlier version of the manuscript. Two reviewers, R. R. Haese and A. P. Roberts, are greatly acknowledged for constructive and detailed comments, which improved the quality of the manuscript. Our special appreciation goes to U. Bleil and H. D. Schulz for helpful discussions. This research was funded by the Deutsche Forschungsgemeinschaft as part of the DFG Research Center "Ocean Margins" of the University of Bremen, No. RCOM0289.

Associate editor: D. E. Canfield

REFERENCES

Adler M., Hensen C., and Schulz H. D. (2000) CoTReM—Column Transport and Reaction Model. User Guide, Version 2.3. http://www.geochemie.uni-bremen.de/cotrem.html.

Adler M., Hensen C., Wenzhöfer F., Pfeifer K., and Schulz H. D. (2001) Modeling of subsurface calcite dissolution by oxic respiration in supralysoclinal deep-sea sediments. *Mar. Geol.* **177,** 167–189.

Aller R. C. and Rude P. D. (1988) Complete oxidation of solid phase sulfides by manganese and bacteria in anoxic marine sediments. *Geochim. Cosmochim. Acta* **52,** 751–765.

Aloisi G., Wallmann K., Drews M., and Bohrmann G. (2004) Evidence for the submarine weathering of silicate minerals in Black Sea sediments: Possible implications for the marine Li and B cycles. *Geochem. Geophys. Geosyst.* **5,** 1–22.

Antoine D., Andre, J.-M. and Morel A. (1996) Oceanic primary production: 2. Estimation at global scale from satellite (coastal zone color scanner) chlorophyll. *Glob. Biogeochem. Cycles* **10,** 57–69.

Archer D. (1996) A data-driven model of the global calcite lysocline. *Glob. Biogeochem. Cycles* **10,** 511–526.

Barnes R. O. and Goldberg E. D. (1976) Methane production and consumption in anoxic marine sediments. *Geology* **4,** 297–300.

Behrenfeld M. J. and Falkowski P. G. (1997) Photosynthetic rates derived from satellite-based chlorophyll concentration. *Limnol. Oceanogr.* **42,** 1–20.

Bernard B. B. (1979) Methane in marine sediments. *Deep-Sea Res.* **26A**, 429–443.

Berner R. A. (1967) Thermodynamic stability of sedimentary iron sulfides. *Am. J. Sci.* **265,** 773–785.

Berner R. A. (1970) Sedimentary pyrite formation. *Am. J. Sci.* **268,** 1–23.

Berner R. A. (1982) Burial of organic carbon and pyrite sulfur in the modern ocean: Its geochemical and environmental significance. *Am. J. Sci.* **282,** 451–473.

Biscaye P. E. and Dasch E. J. (1971) The rubidium, strontium, strontium-isotope system in deep-sea sediments: Argentine Basin. *J. Geophys. Res.* **76,** 5087–5096.

Blair N. E. and Aller R. C. (1995) Anaerobic methane oxidation on the Amazon shelf. *Geochim. Cosmochim. Acta* **59,** 3707–3715.

Bleil U. (2000) Sedimentary magnetism. In *Marine Geochemistry* (eds. H. D. Schulz and M. Zabel). Springer, pp. 73–84.

Bleil U. et al. (2001) Report and preliminary results of *Meteor* cruise M 46/3 Montevideo–Mar del Plata, 04.01.–07.02.2000, *Ber. Fachb. Geowiss. Univ. Bremen* **172**.

Borowski W. S., Paull C. K., and Ussler W. (1996) Marine porewater sulfate profiles indicate in situ methane flux from underlying gas hydrate. *Geology* **24,** 655–658.

Boudreau B. P. (1997) *Diagenetic Models and Their Implementation: Modelling Transport and Reactions in Aquatic Sediments*. Springer.

Butler I. B. and Rickard D. (2000) Framboidal pyrite formation via the oxidation of iron (II) monosulfides by hydrogen sulfide. *Geochim. Cosmochim. Acta* **64,** 2665–2672.

Canfield D. E. and Berner R. A. (1987) Dissolution and pyritization of magnetite in anoxic marine sediments. *Geochim. Cosmochim. Acta* **51,** 645–659.

Canfield D. E. (1989) Reactive iron in marine sediments. *Geochim. Cosmochim. Acta* **53,** 619–632.

Canfield D. E., Raiswell R., and Bottrell S. (1992) The reactivity of sedimentary iron minerals toward sulfide. *Am. J. Sci.* **292,** 659–683.

Channell J. E. T. and Hawthorne T. (1990) Progressive dissolution of titanomagnetites at ODP Site 653 (Tyrrhenian Sea). *Earth Planet. Sci. Lett.* **96,** 469–480.

Channell J. E. T. and Stoner J. S. (2002) Plio-Pleistocene magnetic polarity stratigraphies and diagenetic magnetite dissolution at ODP Leg 177 Sites (1089, 1091, 1093 and 1094). *Mar. Micropal.* **45,** 269–290.

Coleman M. L. and Raiswell R. (1995) Source of carbonate and origin of zonation in pyritiferous carbonate concretions: Evaluation of a dynamic model. *Am. J. Sci.* **295,** 282–308.

de Lange G. J. (1983) Geochemical evidence of a massive slide in the southern Norwegian Sea. *Nature* **305,** 420–422.

Ewing M. and Leonardi A. G. (1971) Sediment transport and distribution in the Argentine Basin. 5. Sedimentary structure of the Argentine margin, basin and related provinces. *Phys. Chem. Earth* **8,** 125–251.

Ewing M., Eittreim S. L., Ewing J. I., and Le Pichon X. (1971) Sediment transport and distribution in the Argentine Basin. 3. Nepheloid layer and processes of sedimentation. *Phys. Chem. Earth* **8,** 51–77.

Ferdelman T. G., Fossing H., Neumann K., and Schulz H. D. (1999) Sulfate reduction in surface sediments of the southeast Atlantic continental margin between 1538′S and 27°57′S (Angola and Namibia). *Limnol. Oceanogr.* **44,** 650–661.

Flood R. D. et al. (1995) *Proc. ODP Init. Repts.* **155**, Ocean Drilling Program.

Frederichs T., Bleil U., Däumler K., von Dobeneck T. and Schmidt A. M. (1999) The magnetic view on the marine paleoenvironment: Parameters, techniques and potentials of rock magnetic studies as a key to paleoclimatic and paleoceanographic changes. In *Use of Proxies in Paleoceanography: Examples from the South Atlantic* (eds. G. Fischer and G. Wefer). Springer, pp. 575–599.

Frenz M., Höppner R., Stuut J.-B. W., Wagner T. and Henrich R. (2003) Surface sediment bulk geochemistry and grain-size composition related to the oceanic circulation along the South American margin in the Southwest Atlantic. In *The South Atlantic in the Late Quaternary: Reconstruction of Material Budget and Current Systems* (eds. G. Wefer, S. Mulitza and V. Ratmeyer). Springer, pp. 347–373.

Froelich P. N., Klinkhammer G. P., Bender M. L., Luedtke N. A., Heath G. R., Cullen D., Dauphin P., Hammond D., Hartman B., and Maynard V. (1979) Early oxidation of organic matter in pelagic sediments of the eastern equatorial Atlantic: Suboxic diagenesis. *Geochim. Cosmochim. Acta* **43,** 1075–1090.

Funk J. A., von Dobeneck T. and Reitz A. (2003a) Integrated rock magnetic and geochemical quantification of redoxomorphic iron mineral diagenesis in Late Quaternary sediments from the Equatorial Atlantic. In *The South Atlantic in the Late Quaternary: Reconstruction of Material Budget and Current Systems* (eds. G. Wefer, S. Mulitza and V. Ratmeyer). Springer, pp. 237–260.

Funk J. A., von Dobeneck T., Wagner T. and Kasten S. (2003b) Late Quaternary sedimentation and early diagenesis in the equatorial Atlantic ocean: Patterns, trends and processes deduced from rock magnetic and geochemical records. In *The South Atlantic in the Late Quaternary: Reconstruction of Material Budget and Current Systems* (eds. G. Wefer, S. Mulitza and V. Ratmeyer). Springer, pp. 461–497.

Furukawa Y. and Barnes H. L. (1995) Reactions forming pyrite from precipitated amorphous ferrous sulfide. In *Geochemical Transformation of Sedimentary Sulfur* (eds. M. A. Vairavamurthy and M. A. A. Schoonen), ACS Symposium Series 612, pp. 194–205.

Garming J. F. L., Bleil U., and Riedinger N. (2005) Alteration of magnetic mineralogy at the sulfate methane transition: Analysis of sediments from the Argentine continental slope. *Phys. Earth Planet. Inter.* **151,** 290–308.

Groot J. J., Groot C. R., Ewing M., Burckle L., and Conolly J. R. (1967) Spores, pollen, diatoms and provenance of the Argentine Basin sediments. *Progr. Oceanogr.* **4,** 179–217.

Haese R. R., Petermann H., Dittert L., and Schulz H. D. (1998) The early diagenesis of iron in pelagic sediments: A multidisciplinary approach. *Earth Planet. Sci. Lett.* **157,** 233–248.

Haese R. R., Schramm J., Rutgers van der Loeff M. M., and Schulz H. D. (2000) A comparative study of iron and manganese diagenesis in continental slope and deep sea basin sediments off Uruguay (SW Atlantic). *Int. J. Earth Sci.* **88,** 619–629.

Harris L. C. and Whiting B. M. (2000) Sequence-stratigraphic significance of Miocene to Pliocene glauconite-rich layers, on- and offshore of the US Mid-Atlantic margin. *Sed. Geol.* **134,** 129–147.

Hensen C., Zabel M., and Schulz H. D. (2000) A comparison of benthic nutrient fluxes from deep-sea sediments off Namibia and Argentina. *Deep-Sea Res. II* **47,** 2029–2050.

Hensen C., Zabel M., Pfeifer K., Schwenk T., Kasten S., Riedinger N., Schulz H. D., and Boetius A. (2003) Control of sulfate pore-water profiles by sedimentary events and the significance of anaerobic oxidation of methane for burial of sulfur in marine sediments. *Geochim. Cosmochim. Acta* **67,** 2631–2647.

Iriondo M. H. (1984) The Quaternary of Northeastern Argentina. In *Quaternary of South America and Antarctic Peninsula* (ed. J. Rabassa) 2. A. A. Balkema, pp. 51–78.

Iversen N. and Jørgensen B. B. (1993) Diffusion coefficients of sulfate and methane in marine sediments: Influence of porosity. *Geochim. Cosmochim. Acta* **57,** 571–578.

Jiang W.-T., Horng C.-S., Roberts A. P., and Peacor D. R. (2001) Contradictory magnetic polarities in sediments and variable timing of neoformation of authigenic greigite. *Earth Planet. Sci. Lett.* **193,** 1–12.

Jørgensen B. B. (1982) Mineralization of organic matter in the sea bed—the role of sulphate reduction. *Nature* **296,** 643–645.

Jørgensen B. B., Böttcher M. E., Lüschen H., Neretin L. N., and Volkov I. I. (2004) Anaerobic methane oxidation and a deep H_2S sink generate isotopically heavy sulfides in Black Sea sediments. *Geochim. Cosmochim. Acta* **68,** 2095–2118.

Kao S.-J., Horng C.-S., Roberts A. P. and Liu, K.-K. (2004) Carbon-sulfur-iron relationships in sedimentary rocks from southwestern Taiwan: Influence of geochemical environment on greigite and pyrrhotite formation. *Chem. Geol.* **203,** 153–168.

Karlin R. and Levi S. (1983) Diagenesis of magnetite minerals in recent hemipelagic sediments. *Nature* **303,** 327–330.

Karlin R. and Levi S. (1985) Geochemical and sedimentological control of the magnetic properties of hemipelagic sediments. *J. Geophys. Res.* **90,** 10373–10392.

Karlin R. (1990) Magnetite diagenesis in marine sediments from the Oregon Continental Margin. *J. Geophys. Res.* **95,** 4405–4419.

Kasten S., Freudenthal T., Gingele F. X., and Schulz H. D. (1998) Simultaneous formation of iron-rich layers at different redox boundaries in sediments of the Amazon deep-sea fan. *Geochim. Cosmochim. Acta* **62,** 2253–2264.

Kasten S., Zabel M., Heuer V. and Hensen C. (2003) Processes and signals of nonsteady-state diagenesis in deep-sea sediments and their pore waters. In *The South Atlantic in the Late Quaternary: Reconstruction of Material Budget and Current Systems* (eds. G. Wefer, S. Mulitza and V. Ratmeyer). Springer, pp. 431–459.

Klaus A. and Ledbetter M. T. (1988) Deep-sea sedimentary processes in the Argentine Basin revealed by high-resolution seismic records (3.5 kHz echograms). *Deep-Sea Res.* **35,** 899–917.

Ledbetter M. T. and Klaus, A. (1987) Influence of bottom currents on sediment texture sea-floor morphology in the Argentine Basin. In *Geology and Geochemistry of Abyssal Plains* (eds. P. P. E. Weaver and J. Thomson), Geological Society of London Special Publication 31, pp. 23–31.

Lovley D. R. (1991) Dissimilatory Fe(III) and Mn(IV) reduction. *Microbiol. Rev.* **55,** 259–287.

Morse J. W. and (Cornwell 1987) Analysis and distribution of iron sulfide minerals in recent anoxic marine sediments. *Mar. Chem.* **22,** 55–69.

Morse J. W. (2002) Sedimentary geochemistry of the carbonate and sulphide systems and their potential influence on toxic metal bioavailability. In *Chemistry of Marine Water and Sediments* (eds. A. Gianguzza, E. Pelizzetti and S. Sammartano). Springer, pp. 165–189.

Neretin L. N., Böttcher M. E., Jørgensen B. B., Volkov I. I., Lüschen H., and Hilgenfeldt K. (2004) Pyritization processes and greigite formation in the advancing sulfidization front in the Upper Pleistocene sediments of the Black Sea. *Geochim. Cosmochim. Acta* **68,** 2081–2093.

Niewöhner C., Hensen C., Kasten S., Zabel M., and Schulz H. D. (1998) Deep sulfate reduction completely mediated by anaerobic methane oxidation in sediments of the upwelling area off Namibia. *Geochim. Cosmochim. Acta* **62,** 455–464.

Odin G. S. and Matter A. (1981) De glauconiarum origine. *Sedimentology* **28,** 611–641.

Passier H. F., Dekkers M. J., and de Lange G. J. (1998) Sediment chemistry and magnetic properties in an anomalously reducing core from the eastern Mediterranean Sea. *Chem. Geol.* **152,** 287–306.

Peterson R. G. and Stramma L. (1991) Upper-level circulation in the South Atlantic Ocean. *Progr. Oceanogr.* **26,** 1–73.

Piccolo M. C. and Perillo G. M. E. (1999) The Argentina estuaries: A review. In *Estuaries of South America* (eds. G. M. E. Perillo, M. C. Piccolo and M. Pino-Quivira). Springer, pp. 101–132.

Postma D. and Appelo C. A. J. (2000) Reduction of Mn-oxides by ferrous iron in a flow system: Column experiment and reactive transport modelling. *Geochim. Cosmochim. Acta* **64,** 1237–1247.

Pyzik A. J. and Sommer S. E. (1981) Sedimentary iron monosulfides: Kinetics and mechanism of formation. *Geochim. Cosmochim. Acta* **45,** 687–698.

Reitz A., Hensen C., Kasten S., Funk J. A., and de Lange G. J. (2004) A combined geochemical and rock-magnetic investigation of a redox horizon at the last glacial/interglacial transition. *Phys. Chem. Earth.* **29,** 921–931.

Rickard D., Schoonen, M. A. A., and Luther G. W. (1995) Chemistry iron in sedimentary environments. In *Geochemical Transformation of Sedimentary Sulfur* (eds. M. A. Vairavamurthy and M.A.A. Schoonen), ACS Symposium Series 612, pp. 168–193.

Rickard D. (1997) Kinetics of pyrite formation by the H_2S oxidation of iron (II) monosulfides in aqueous solutions between 25 and 125°C: The rate equation. *Geochim. Cosmochim. Acta* **61,** 115–134.

Roberts A. P. and Turner G. M. (1993) Diagenetic formation of ferrimagnetic iron sulphide minerals in rapidly deposited marine sediments, South Island, New Zealand. *Earth Planet. Sci. Lett.* **115,** 257–273.

Romero O. and Hensen C. (2002) Oceanographic control of biogenic opal and diatoms in surface sediments of the South Western Atlantic. *Mar. Geol.* **186,** 263–280.

Sachs S. D. and Ellwood B. B. (1988) Controls on magnetic grain size variations and concentration in the Argentine Basin, South Atlantic Ocean. *Deep-Sea Res.* **35,** 929–942.

Schippers A. and Jørgensen B. B. (2001) Oxidation of pyrite and iron sulfide by manganese dioxide in marine sediments. *Geochim. Cosmochim. Acta* **65,** 915–922.

Schneider R., Probst U., and Donner B. (1991) Stratigraphie. Bericht und Erste Ergebnisse der *Meteor*-Fahrt M 16/2, Recife–Belem, 28.04.–21.05.1991. *Ber. Fachb. Geowiss. Univ. Bremen* **19,** 51–67.

Schoonen M. A. A. and Barnes H. L. (1991) Reactions forming pyrite and marcasite from solution: II. Via FeS precursors below 100°C. *Geochim. Cosmochim. Acta* **55,** 1505–1514.

Schulz H. D. et al (2001) Report and preliminary results of *Meteor* cruise M 46/2 Recife–Montevideo, 02.12.–29.12.1999. *Ber. Fachb. Geowiss. Univ. Bremen* **174**.

Schulz H. D. (2000) Quantification of early diagenesis: Dissolved constituents in marine pore water. In *Marine Geochemistry* (eds. H. D. Schulz and M. Zabel). Springer, pp. 85–128.

Tarduno J. A. and Wilkison S. L. (1996) Non-steady state magnetic mineral reduction, chemical lock-in and delayed remanence acquisition in pelagic sediments. *Earth Planet. Sci. Lett.* **144,** 315–326.

Wilson T. R. S., Thomson J., Hydes D. J., Colley S., Culkin F., and Sørensen J. (1986) Oxidation fronts in pelagic sediments: Diagenetic formation of metal-rich layers. *Science* **232,** 972–975.

Vogt C., Lauterjung J., and Fischer R. X. (2002) Investigation of the clay fraction (<2 μm) of the Clay Minerals Society reference clays. *Clays Clay Minerals* **50,** 388–400.

Zabel M. and Schulz H. D. (2001) Importance of submarine landslides for non-steady state conditions in pore water systems. *Mar. Geol.* **176,** 87–99.